Hindawi
Mobile Information Systems
Volume 2022, Article ID 4361155, 13 pages
https://doi.org/10.1155/2022/4361155

Research Article

A Novel Countermeasure Method for Radar Coherent Jamming Based on Signal Feature Transformation

Zhipeng Liu, Ningning Jia, Yuntian Feng, Baojie Hu, Xiaoyang Wang, Yanyang Gu, and Zhipeng Fan

State Key Laboratory of Complex Electromagnetic Environment Effects on Electronics and Information System, Luoyang, China

Correspondence should be addressed to Zhipeng Liu; liuzhip1994@163.com

Received 23 April 2022; Revised 30 October 2022; Accepted 25 November 2022; Published 8 December 2022

Academic Editor: Zahid Mehmood

With the advancement of active jamming technology, a variety of new types of coherent jamming based on digital radio frequency memory (DFRM) have been proposed and implemented in practice, posing serious threats to modern radar systems due to their flexibility, suppression, and deception characteristics. Hence, the research on relevant countermeasures is necessary and challenging. In this paper, we take a fresh look at the problem and present a method for removing interference from received time-frequency overlapping signals based on signal feature modification (SFT). The antijamming problem is transformed into one linear underdetermined blind source separation (UBSS) model in a dual-channel receiving scenario using sparse component analysis, and the feasible solution is found by transforming the observed signal features to a new time-frequency domain representation. Simulations demonstrate that the developed technique outperforms standard interference countermeasures in terms of signal-to-interference ratio (SIR) and target identification performance, which are critical for antijamming.

1. Introduction

The electromagnetic jamming and countermeasure technology of radar systems have long been the research hotspots and roadblocks in modern electronic warfare. Up to now, active jamming technology has advanced from noise suppression to widespread usage of coherent jamming, such as range and speed gate pull off. As a result of the rapid development of digital radio frequency memory (DRFM) technology, new types of coherent jamming have emerged, such as noise convolution jamming, slice jamming, and interrupted-sampling jamming [1], which easily create severe overlaps with target echoes in time and frequency domain. Due to the suppression and deception features of contemporary coherent jamming, the working modes are extremely flexible, significantly reducing the performance of modern radar systems.

Antijamming is all about extracting the different features between the interfering signal and the target signal and then eliminating the interference based on these different features to highlight the target signal's amplitude following pulse compression. The new coherent jamming exhibits a strong correlation with the target echo, which could cause critical time and frequency domain overlaps with the echo if the parameters inside the adjacent pulse repetition intervals (PRIs) remain constant. Particularly, the difference extraction may be harder when the signal-to-interference ratio (SIR) and signal-to-noise ratio are low (SNR).

From the perspective of polarization characteristics, the authors of [2, 3] build polarization filters in radar transceiver systems to make the polarization mode of target echo orthogonal to interference, while this method is only applicable to multipolarization radar and has a high computational cost. In [4, 5], certain optimization methods based on adaptive beamforming are used, and their fundamental limitation is that the main beam may occasionally suffer severe distortion, significantly impairing the subsequent target detection and parameter estimation performance. References [6, 7] propose extracting the difference features following phase quantization, and it obtains obvious effectiveness only in a limited number of application scenarios. There are also several approaches based on frequency

agility and waveform diversity in references [8, 9], but they typically require a substantial amount of radar internal resources and have undesirable effects.

Recently, the methods based on sparse component analysis (SCA) have been proven to be an excellent solution for radar antijamming, which approximately consist of two steps: (1) the estimation of the observed mixing matrix; (2) the separation and recovery of the target echo using the estimated mixing matrix. Although the matrix estimation technique based on observed signals is rather established [10, 11], the separation and recovery method of target echo remains a research hotspot. The orthogonal matching pursuit based on a greedy or distinct sampling strategy in the time-frequency domain has been advocated in [12, 13], and in these papers, the primary components of the target signal are extracted successively to recover the main signal features of the target echo. In [14, 15], the convex optimization methods are utilized to obtain a sparser representation of the observed signal model by determining the minimum of l_1 norm or approximate l_0 norm. However, the approaches described above perform well only when input signals are extremely sparse, which indicates that their performance and stability cannot be guaranteed during actual radar signal receiving.

To address the target echo extraction problem and alleviate the sparsity constraint on input hybrid signals, we propose a novel separation method based on signal feature transformation (SFT) in a dual-channel reception scenario. This method is applicable to multiple-input multiple-output (MIMO) or multiple-input single-output (MISO) digital programmable radar systems, and the pipeline is shown in Figure 1. The heart of it is to transform the radar antijamming problem to one linear underdetermined blind source separation (UBSS) model and then to use SFT to obtain new features from the observed signals in the time-frequency domain. Finally, the model is solved using basic screening to achieve target echo separation and recovery.

The rest of the paper is structured as follows. In Section 2, a dual-channel time-frequency overlapped signal model is introduced, and the proposed method is described. Section 3 briefly gives the explication of simulation data, and the performance of the proposed method is verified and compared with traditional methods. Conclusions are drawn in Section 4.

2. The Proposed Method

2.1. Signal Model. Here, the dual-channel receiving hybrid signal is described as a linear UBSS model as follows:

$$\begin{aligned}\mathbf{f}(t) &= \begin{bmatrix} f_1(t) \\ f_2(t) \end{bmatrix} \\ &= \begin{bmatrix} a_{11} & a_{12} & \cdots & a_{1n} \\ a_{21} & a_{22} & \cdots & a_{2n} \end{bmatrix} \begin{bmatrix} s_1(t) \\ s_2(t) \\ \vdots \\ s_n(t) \end{bmatrix} + \mathbf{v}(t) \\ &= \mathbf{A}\mathbf{s}(t) + \mathbf{v}(t), \\ t &= 1, 2, \ldots, T, \end{aligned} \tag{1}$$

where $\mathbf{f}(t)$ and $\mathbf{s}(t)$ denote the observed signals and sources (target echo and interfering signals), respectively, $\mathbf{A} \in R^{2\times n}$ denotes the observed mixing matrix, and $\mathbf{v}(t)$ models the additive Gaussian noise. As indicated previously, due to the time-frequency overlaps, $\mathbf{f}(t)$ exhibits poor sparsity, and the conventional filtering and positive definite blind source separation methods (e.g., joint diagonalization and fixed-point methods) are incapable of achieving effective separation [16–18]. To increase the signal sparsity, here, $\mathbf{f}(t)$ is converted to time-frequency domain for processing; that is,

$$\begin{aligned}\mathbf{F}(t,f) &= \begin{bmatrix} F_1(t,f) \\ F_2(t,f) \end{bmatrix} \\ &= \begin{bmatrix} a_{11} & a_{12} & \cdots & a_{1n} \\ a_{21} & a_{22} & \cdots & a_{2n} \end{bmatrix} \begin{bmatrix} S_1(t,f) \\ S_2(t,f) \\ \vdots \\ S_n(t,f) \end{bmatrix} + \mathbf{V}(t,f) \\ &= \mathbf{A}\mathbf{S}(t,f) + \mathbf{V}(t,f), \end{aligned} \tag{2}$$

where $\mathbf{F}(t,f)$, $\mathbf{S}(t,f)$, and $\mathbf{V}(t,f)$ are matrices of the time-frequency coefficient of $\mathbf{f}(t)$, $\mathbf{s}(t)$, and $\mathbf{v}(t)$, respectively. Here, a single time-frequency coefficient is referred to as a time-frequency point (TF point).

Prior to source separation, the observed mixing matrix estimation is considered. In this paper, we employ the estimate method described in [10], which enables estimation to be completed without previous knowledge of the number of sources, while maintaining a stable accuracy that can be regulated by the size of the probability interval. Notably, the size of the estimated matrix $\widehat{\mathbf{A}}$ is typically larger than the true mixing matrix $\mathbf{A}$, and the column vectors are enlarged to provide some virtual sources, which adds some computational overhead but has no effect on the separation performance. Following the observed matrix estimation, given $\mathbf{F}(t,f)$, the task is to extract the time-frequency features of the target echo. Following that, the method is described in detail as follows.

2.2. Target Echo Extraction Based on SFT. The required assumptions are made here to make hybrid signals separable.

Assumption 1. Any submatrix of size 2×2 decomposed from the observed matrix $\mathbf{A} \in R^{2\times n}$ is nonsingular, which means any two columns are independent of each other.

Assumption 1 ensures the separability of the observed signal, which is a critical premise of the approach provided in this study. Given the random nature of signal energy attenuation in various transmission routes in practice, Assumption 1 is widely accepted [18].

To facilitate analysis, here, the size of $\mathbf{A}$ is set as 2×3, indicating that three sources are mixed in two received hybrid signals, and $\mathbf{v}(t) = 0$. The observed matrix $\mathbf{A} \in R^{2\times 3}$ is represented as follows:

$$\mathbf{A} = \begin{bmatrix} a_{11} & a_{12} & a_{13} \\ a_{21} & a_{22} & a_{23} \end{bmatrix}. \tag{3}$$

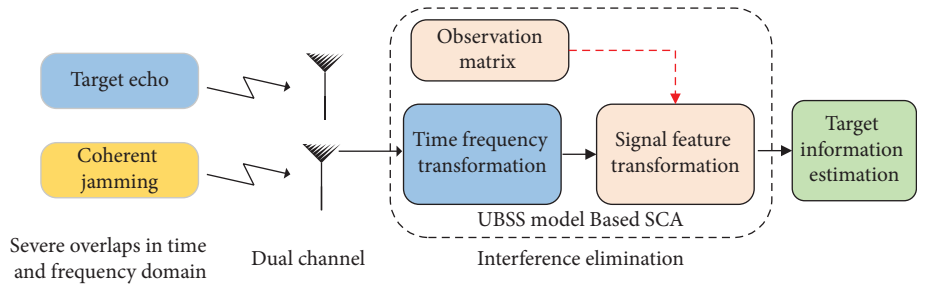

Figure 1: The pipeline of the proposed method.

As a result of the singularity of $\mathbf{A}$, its inverse matrix is pseudoinverse $\mathbf{A}^{+}$ while the inaccuracy $\{\mathbf{E}_3 - \mathbf{A}^{+}\mathbf{A}\}$ is excessive for practical purposes, where $\mathbf{E}_3$ denotes the third-order identity matrix. Thus, the nonsingular matrices of size 2×2 decomposed from $\mathbf{A}$ are considered, which are [19]

$$\begin{aligned}\mathbf{A}^{12} &= \begin{bmatrix} a_{11} & a_{12} \\ a_{21} & a_{22} \end{bmatrix}, \\ \mathbf{A}^{13} &= \begin{bmatrix} a_{11} & a_{13} \\ a_{21} & a_{23} \end{bmatrix},\end{aligned} \tag{4}$$

and the corresponding inverse matrices are

$$\begin{aligned}\mathbf{A}_{inv}^{12} &= \frac{1}{a_{11}a_{22} - a_{12}a_{21}} \begin{bmatrix} a_{22} & -a_{12} \\ -a_{21} & a_{11} \end{bmatrix}, \\ \mathbf{A}_{inv}^{13} &= \frac{1}{a_{11}a_{23} - a_{13}a_{21}} \begin{bmatrix} a_{23} & -a_{13} \\ -a_{21} & a_{11} \end{bmatrix}.\end{aligned} \tag{5}$$

Because $\mathbf{A}_{inv}^{12} \cdot \mathbf{A}^{12} = \mathbf{E}_2$, $\mathbf{A}_{inv}^{13} \cdot \mathbf{A}^{13} = \mathbf{E}_2$, then

$$\begin{aligned}\mathbf{A}_p^{12} &= \mathbf{A}_{inv}^{12} \cdot \mathbf{A} \\ &= \begin{bmatrix} 1 & 0 & \dfrac{a_{22}a_{13} - a_{12}a_{23}}{a_{11}a_{22} - a_{12}a_{21}} \\ 0 & 1 & \dfrac{a_{11}a_{23} - a_{13}a_{21}}{a_{11}a_{22} - a_{12}a_{21}} \end{bmatrix} \\ &= \begin{bmatrix} 1 & 0 & \beta_{13}^{12} \\ 0 & 1 & \beta_{23}^{12} \end{bmatrix},\end{aligned} \tag{6}$$

$$\begin{aligned}\mathbf{A}_p^{13} &= \mathbf{A}_{inv}^{13} \cdot \mathbf{A} \\ &= \begin{bmatrix} 1 & \dfrac{a_{12}a_{23} - a_{13}a_{22}}{a_{11}a_{23} - a_{13}a_{21}} & 0 \\ 0 & \dfrac{a_{11}a_{22} - a_{12}a_{21}}{a_{11}a_{23} - a_{13}a_{21}} & 1 \end{bmatrix} \\ &= \begin{bmatrix} 1 & \beta_{12}^{13} & 0 \\ 0 & \beta_{22}^{13} & 1 \end{bmatrix},\end{aligned} \tag{7}$$

where β_{13}^{12}, β_{23}^{12}, β_{12}^{13}, and β_{22}^{13} are nonzero values. Considering (6) and (7), the time-frequency features $\mathbf{F}(t, f)$ are transformed to new representations that can be theoretically characterized as

$$\begin{aligned}\mathbf{F}^{12}(t, f) &= \mathbf{A}_{inv}^{12}\mathbf{F}(t, f) \\ &= \mathbf{A}_p^{12}\mathbf{S}(t, f), \\ \mathbf{F}^{13}(t, f) &= \mathbf{A}_{inv}^{13}\mathbf{F}(t, f) \\ &= \mathbf{A}_p^{13}\mathbf{S}(t, f),\end{aligned} \tag{8}$$

where $\mathbf{F}^{12}(t, f)$ and $\mathbf{F}^{13}(t, f)$ are the new representations of the observation information under $\mathbf{A}^{12}$ and $\mathbf{A}^{13}$, which can be expanded as follows:

$$\begin{aligned}\mathbf{F}^{12}(t, f) &= \begin{bmatrix} F_1^{12}(t, f) \\ F_2^{12}(t, f) \end{bmatrix} \\ &= \mathbf{A}_p^{12} \begin{bmatrix} S_1(t, f) \\ S_2(t, f) \\ S_3(t, f) \end{bmatrix} \\ &= \begin{bmatrix} S_1(t, f) + \beta_{13}^{12} S_3(t, f) \\ S_2(t, f) + \beta_{23}^{12} S_3(t, f) \end{bmatrix},\end{aligned} \tag{9}$$

$$\begin{aligned}\mathbf{F}^{13}(t, f) &= \begin{bmatrix} F_1^{13}(t, f) \\ F_2^{13}(t, f) \end{bmatrix} \\ &= \mathbf{A}_p^{13} \begin{bmatrix} S_1(t, f) \\ S_2(t, f) \\ S_3(t, f) \end{bmatrix} \\ &= \begin{bmatrix} S_1(t, f) + \beta_{12}^{13} S_2(t, f) \\ S_3(t, f) + \beta_{22}^{13} S_2(t, f) \end{bmatrix}.\end{aligned} \tag{10}$$

As illustrated in (9) and (10), S_2 and S_3 are eliminated from $F_1^{12}(t, f)$ and $F_1^{13}(t, f)$, respectively. For a purer target echo, additional extraction work is required. Let (t_1, f_1) denotes the position of TF points of S_1, and it means that $S_1(t_1, f_1) \neq 0$, and $S_2(t_1, f_1) = S_3(t_1, f_1) = 0$. To find (t_1, f_1), here, the conclusion is given in advance and illustrated as

$$\begin{aligned} &F_2^{12}(t_1, f_1) = F_2^{13}(t_1, f_1) = 0, \\ &\quad\updownarrow \\ &S_2(t_1, f_1) = S_3(t_1, f_1) = 0, F_1^{12}(t_1, f_1) \\ &\quad = F_1^{13}(t_1, f_1) = S_1(t_1, f_1). \end{aligned} \tag{11}$$

Here, the sufficiency and necessity of (11) are proved as follows. The sufficiency is

$$\begin{aligned} &S_2(t_1, f_1) = S_3(t_1, f_1) = 0, \\ &\quad\downarrow \\ &F_2^{12}(t_1, f_1) = S_2(t_1, f_1) + \beta_{23}^{12} S_3(t_1, f_1) = 0, \\ &F_2^{13}(t_1, f_1) = S_3(t_1, f_1) + \beta_{22}^{13} S_2(t_1, f_1) = 0. \end{aligned} \tag{12}$$

About the necessity, if $F_2^{12}(t_1, f_1) = F_2^{13}(t_1, f_1) = 0$, the result can be

$$\begin{aligned} &S_2(t_1, f_1) + \beta_{23}^{12} S_3(t_1, f_1) = S_3(t_1, f_1) + \beta_{22}^{13} S_2(t_1, f_1) = 0, \\ &\left(1 - \beta_{22}^{13}\right) S_2(t_1, f_1) = \left(1 - \beta_{23}^{12}\right) S_3(t_1, f_1). \end{aligned} \tag{13}$$

Let $y \in R$, $y \neq \beta_{22}^{13}$, $y \neq \beta_{23}^{12}$, and (13) can be

$$\begin{aligned} &y\left[S_2(t_1, f_1) + \beta_{23}^{12} S_3(t_1, f_1)\right] = S_3(t_1, f_1) + \beta_{22}^{13} S_2(t_1, f_1) = 0, \\ &\quad\downarrow \\ &\left(y - \beta_{22}^{13}\right) S_2(t_1, f_1) = \left(1 - y\beta_{23}^{12}\right) S_3(t_1, f_1). \end{aligned} \tag{14}$$

Therefore, $\left(y - \beta_{22}^{13}\right) S_2(t_1, f_1) = \left(1 - y\beta_{23}^{12}\right) S_3(t_1, f_1) \equiv 0$ is always established. If $y = 1$, then

$$\left(1 - \beta_{22}^{13}\right) S_2(t_1, f_1) = \left(1 - \beta_{23}^{12}\right) S_3(t_1, f_1) = 0. \tag{15}$$

Suppose that $1 - \beta_{22}^{13} = 1 - \beta_{23}^{12} = 0$, and then, $\beta_{22}^{13} = \beta_{23}^{12} = 1$. According to (6) and (7), it can be seen that

$$\frac{a_{11}a_{22} - a_{12}a_{21}}{a_{11}a_{23} - a_{13}a_{21}} = \frac{a_{11}a_{23} - a_{13}a_{21}}{a_{11}a_{22} - a_{12}a_{21}} = 1, \tag{16}$$

and (16) is simplified to

$$\frac{a_{21}}{a_{11}} = \frac{c\left(a_{23} - a_{22}\right)}{c\left(a_{13} - a_{12}\right)} \longrightarrow \begin{cases} a_{22} = a_{23} - \dfrac{a_{21}}{c}, \\ \\ a_{12} = a_{13} - \dfrac{a_{11}}{c}, \end{cases} \tag{17}$$

where $c \in R$. Here, we set $\beta_{13}^{12} = k, k \in R$, and

$$\frac{a_{22}a_{13} - a_{12}a_{23}}{a_{11}a_{22} - a_{12}a_{21}} = k \longrightarrow \frac{a_{12}}{a_{22}} = \frac{a_{13} - ka_{11}}{a_{23} - ka_{21}}. \tag{18}$$

From (17) and (18), it can be known that $\beta_{13}^{12} = 1/c$. In the same way, $\beta_{12}^{13} = -1/c$; thus, $\beta_{13}^{12} + \beta_{12}^{13} = 0$, which is expressed as

$$\begin{aligned} \beta_{13}^{12} + \beta_{12}^{13} &= \frac{a_{22}a_{13} - a_{12}a_{23}}{a_{11}a_{22} - a_{12}a_{21}} + \frac{a_{12}a_{23} - a_{13}a_{22}}{a_{11}a_{23} - a_{13}a_{21}} \\ &= \frac{\left(a_{22}a_{13} - a_{12}a_{23}\right)\left(a_{11}a_{23} - a_{13}a_{21}\right) + \left(a_{12}a_{23} - a_{13}a_{22}\right)\left(a_{11}a_{22} - a_{12}a_{21}\right)}{\left(a_{11}a_{22} - a_{12}a_{21}\right)\left(a_{11}a_{23} - a_{13}a_{21}\right)} \\ &= \frac{a_{11}a_{13}a_{22}\left(a_{23} - a_{22}\right) + a_{13}a_{21}a_{22}\left(a_{12} - a_{13}\right) + a_{11}a_{12}a_{23}\left(a_{22} - a_{23}\right) + a_{12}a_{21}a_{23}\left(a_{13} - a_{12}\right)}{\left(a_{11}a_{22} - a_{12}a_{21}\right)\left(a_{11}a_{23} - a_{13}a_{21}\right)} \\ &= \frac{\left[a_{11}\left(a_{23} - a_{22}\right) + a_{21}\left(a_{12} - a_{13}\right)\right]\left(a_{13}a_{22} - a_{12}a_{23}\right)}{\left(a_{11}a_{22} - a_{12}a_{21}\right)\left(a_{11}a_{23} - a_{13}a_{21}\right)}. \end{aligned} \tag{19}$$

According to Assumption 1, any two columns are independent of each other in **A**; hence, $(a_{13}a_{22} - a_{12}a_{23})$ is nonzero, and $a_{11}(a_{23} - a_{22}) = a_{21}(a_{12} - a_{13}) = 0$ is also unable to hold. Therefore, $\beta_{13}^{12} + \beta_{12}^{13} \neq 0$, which means $\beta_{22}^{13} \neq 1, \beta_{23}^{12} \neq 1$, and (15) is established if and only if $S_2(t_1, f_1) = S_3(t_1, f_1) = 0$. Taking into account the noise and the operability in practice, (11) is rewritte1 as

$$\begin{aligned} &\begin{cases} |F_2^{12}(t_1, f_1)| < \varepsilon_1, \\ |F_2^{13}(t_1, f_1)| < \varepsilon_1, \end{cases} \\ &\quad\updownarrow \\ &F_1^{12}(t_1, f_1) = F_1^{13}(t_1, f_1) = S_1(t_1, f_1), \end{aligned} \tag{20}$$

where $\varepsilon_1 \leq 0.1$. Let Ω_1 denotes a set of extracted $S_1(t_1, f_1)$, since the filtering of ε_1, and then Ω_1 always contains the TF

Table 1: The related parameters of transmitted signal and interfering signal.

Type	Signal frequency (MHz)	Bandwidth (MHz)	Duration (μs)	Pulse repetition frequency (Hz)	Repeater delay
		Sampling frequency $Fs = 20$ (MHz)			
Transmitted signal	4	3	30	3000	—
Noise convolution jamming					2 μs, 20 μs
Slicing jamming					3 μs, 20 μs
Interrupted sampling and repeater jamming					3 μs, 20 μs

points of other sources and noise. Therefore, to get an improved extraction, the minimum energy principle (MEP) is adopted to optimize Ω_1. According to (9) and (10), the energy of $F_1^{12}(t_1, f_1)$ and $F_1^{13}(t_1, f_1)$ can be expressed as

$$\begin{aligned} Q\left(F_1^{12}(t,f)\right) &= 1 + \left|\beta_{13}^{12}\right|, \\ Q\left(F_1^{13}(t,f)\right) &= 1 + \left|\beta_{12}^{13}\right|, \end{aligned} \tag{21}$$

where $Q(\cdot)$ is the energy-extracting function. To minimize the influence of other sources on S_1 as much as possible, the target with a smaller value of Q is selected as Ω_1. So far, the time-frequency features of S_1 are extracted, and S_2 and noise S_3 are effectively eliminated. For better comparison, inverse STFT (ISTFT) can be applied on Ω_1 to get the time domain signal sequence.

Due to the lack of prior information, the relationship between the target echo and the column in $\mathbf{A}$ is ambiguous, and it is necessary to extract all the nonsingular submatrices $\mathbf{A}^{ij}$ to determine the target echo.

Similarly, according to the above process, the extraction of signal features of S_2 and S_3 can be completed through different nonsingular matrices, and the corresponding relations are listed as follows:

$$\begin{aligned} \left\{\mathbf{A}^{21}, \mathbf{A}^{23}\right\} &\longrightarrow \Omega_2 \longrightarrow S_2, \\ \left\{\mathbf{A}^{31}, \mathbf{A}^{32}\right\} &\longrightarrow \Omega_3 \longrightarrow S_3. \end{aligned} \tag{22}$$

Now, we're going to generalize the process to $\mathbf{A} \in R^{2\times N}$, and then, $\mathbf{A}^{ij}$ is

$$\begin{aligned} &\mathbf{A}^{ij} = \begin{bmatrix} a_{1i} & a_{1j} \\ a_{2i} & a_{2j} \end{bmatrix} (1 \le i, j \le N, i \ne j), \\ &\left\{\mathbf{A}^{i1}, \mathbf{A}^{i2}, \ldots, \mathbf{A}^{i(i-1)}, \mathbf{A}^{i(i+1)}, \ldots, \mathbf{A}^{iN}\right\} \longrightarrow \Omega_i \longrightarrow S_i. \end{aligned} \tag{23}$$

Let Ω_i denotes the set of TF points of S_i, ant its extraction can be expressed as

$$\begin{cases} H = [1, 2, \cdots, i-1, i+1, \cdots N], \\ \left|F_2^{ij}(t_i, f_i)\right| < \varepsilon_1, \forall j \in H, \\ \Omega_i = F_1^{ik}(t_i, f_i), k = \underset{k\in H}{\arg\min}\, Q\left(F_1^{ik}(t_i, f_i)\right), \\ S_i(t_i, f_i) \in \Omega_i. \end{cases} \tag{24}$$

3. Results and Analysis

3.1. Data Preparation. Here, the pulse signal with the linear frequency modulation (LFM) is utilized as the received signal in our simulation, and four types of coherent interfering signals are introduced, which are noise convolution jamming, slicing jamming, and interrupted-sampling and repeater jamming (ISRJ), where ISRJ contains two modes: direct repeater and repeating repeater.

In the simulation, we cut out the received signals and limit them to one PRI, and the signals are converted by the frequency down conversion. All the subsequent processing is made in the baseband, and the related parameters are shown in Table 1. Here, we add two interfering signals on echo with different repeater delays for each type, and the sampling strategy in slice jamming and ISRJ is one-tenth of the echo signal length.

Here, two tests are needed. The purpose of test 1 is to verify the validity and effectiveness of the proposed method under selected interfering signal types, and the details and results of the interference elimination are described. In test 2, two interference countermeasure methods are added to make a comparison for illustrating the superiority of the proposed method.

3.2. Test 1. The radial distance between the target and the radar is set as 20 km. The radar receiver works with dual-channel, and the received signal is a time-frequency overlapped signal made up of target echo, interfering signal (SIR = −15 dB), and random noise (SNR = 0 dB). In the liner separation model, the size of observed mixing matrix $\mathbf{A}$ is 2×3, and here, we set it as a random array greater than 0 which obeys the uniform distribution.

Following the parameters in Table 1, the spectrums and time-frequency distributions of the hybrid signals are given, respectively, in Figure 2. It can be seen that the echoes are completely submerged in different interfering signals, which are hard to get any available information.

After the extraction, the time-frequency distribution of the target echo gets revealed, and the inverse STFT and pulse compression before and after processing are also added for verification, as shown in Figure 3. To quantify the eliminating performance, the results before and after interference elimination are shown in Table 2, which contain the SIR, the error rate of estimated radial distance, and the estimated target number, and the target

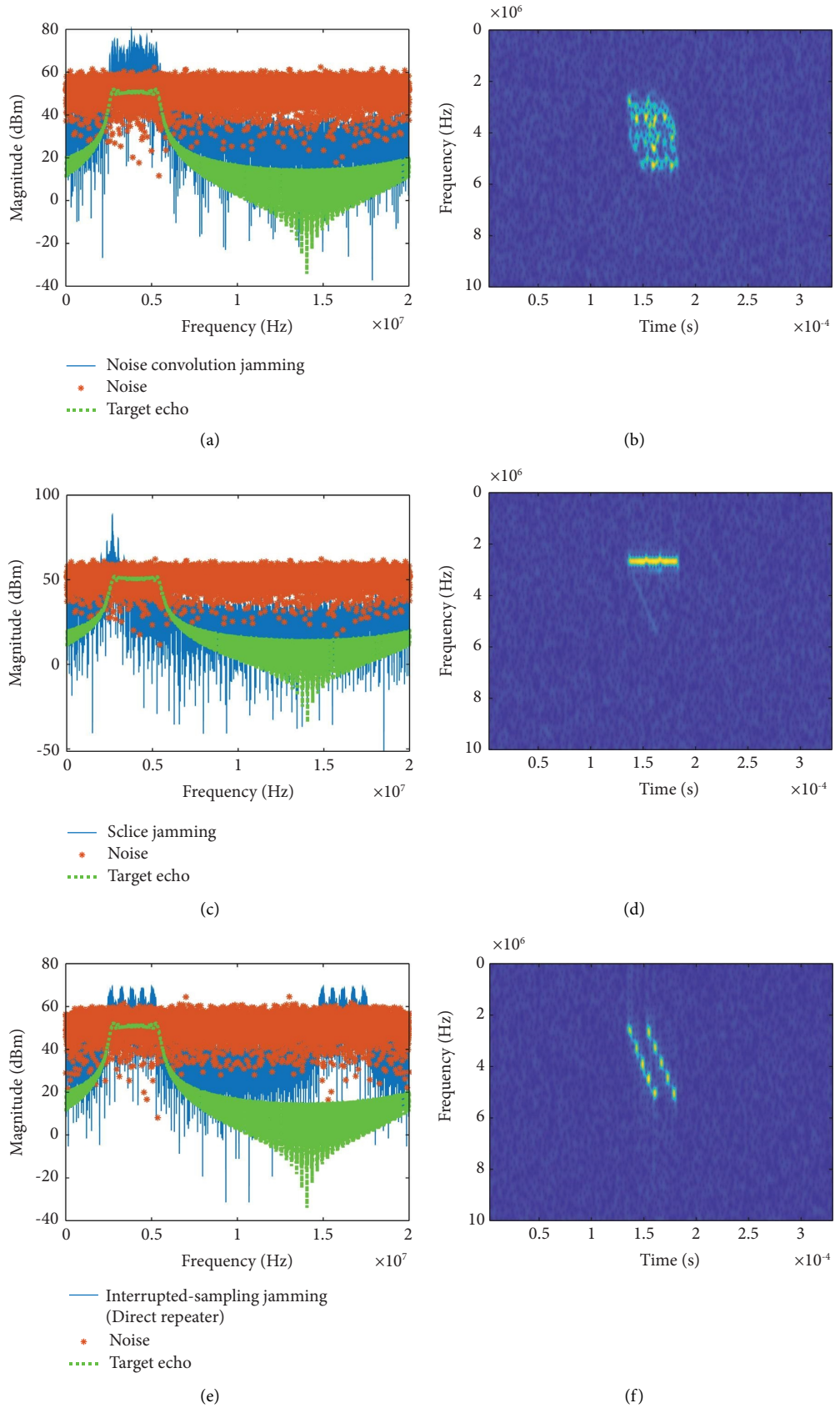

Figure 2: Continued.

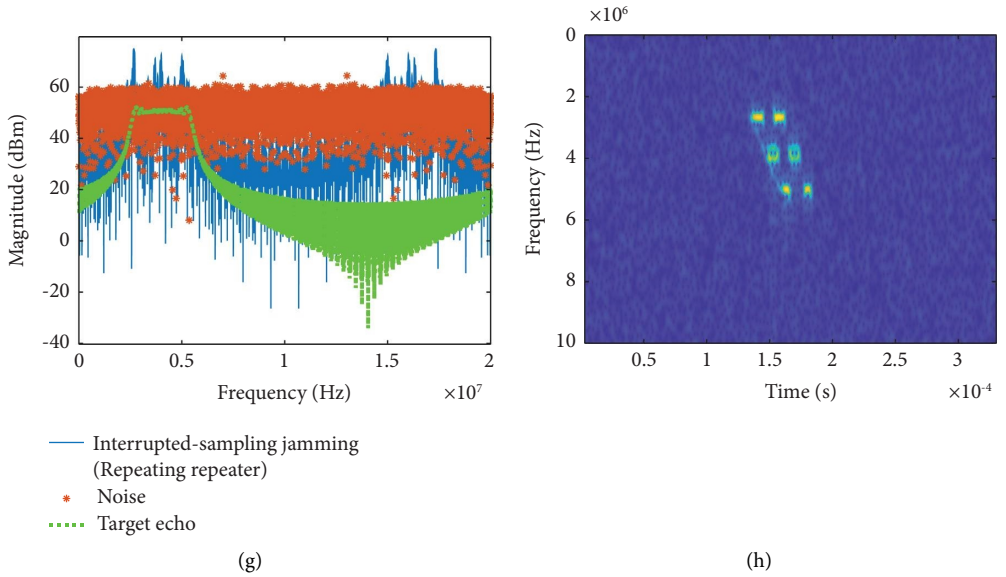

Figure 2: The spectrums and time-frequency distributions of hybrid received signals. (a, b) Noise convolution jamming; (c, d) slicing jamming; (e, f) ISRJ-direct repeater; (g, h) ISRJ-repeating repeater (SIR = −15 dB, SNR = 0 dB).

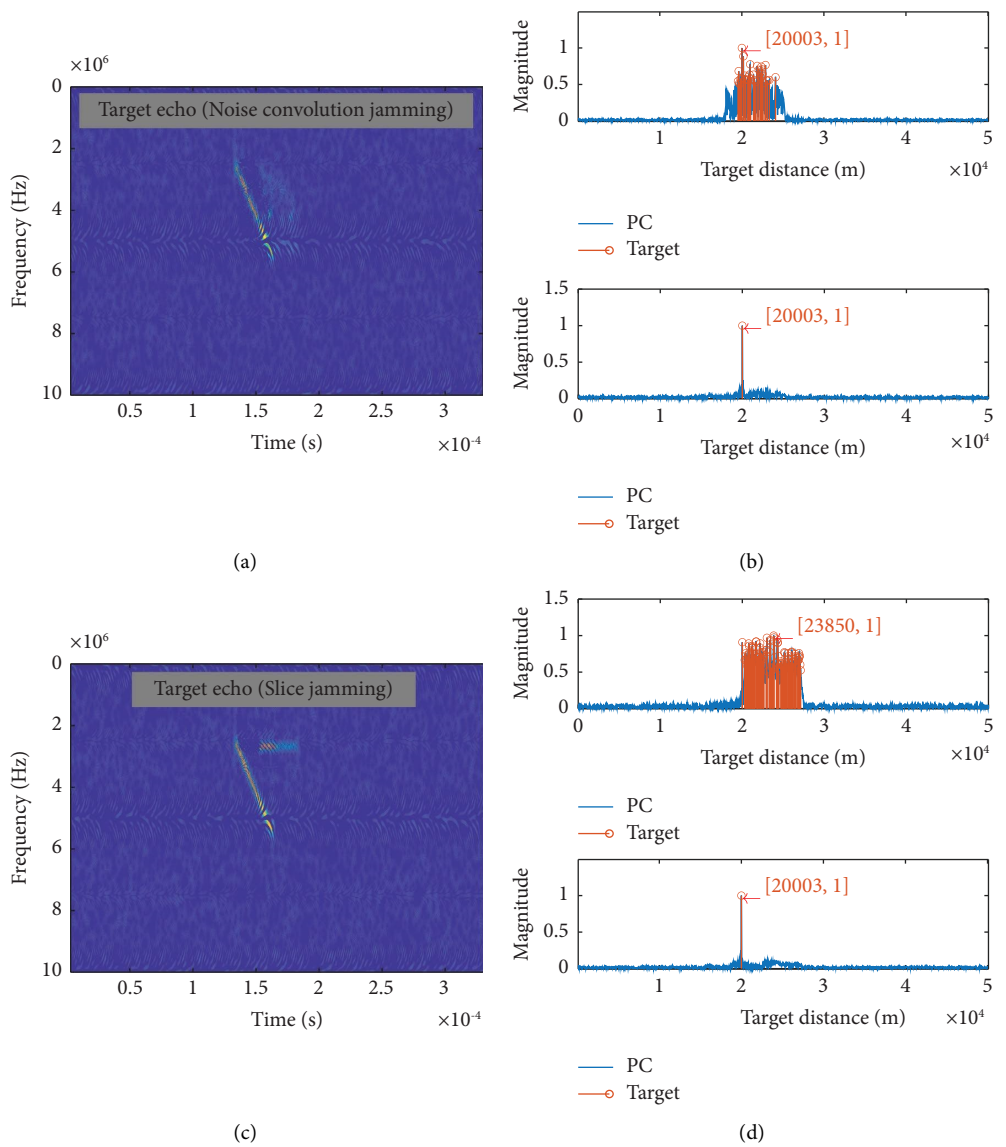

Figure 3: Continued.

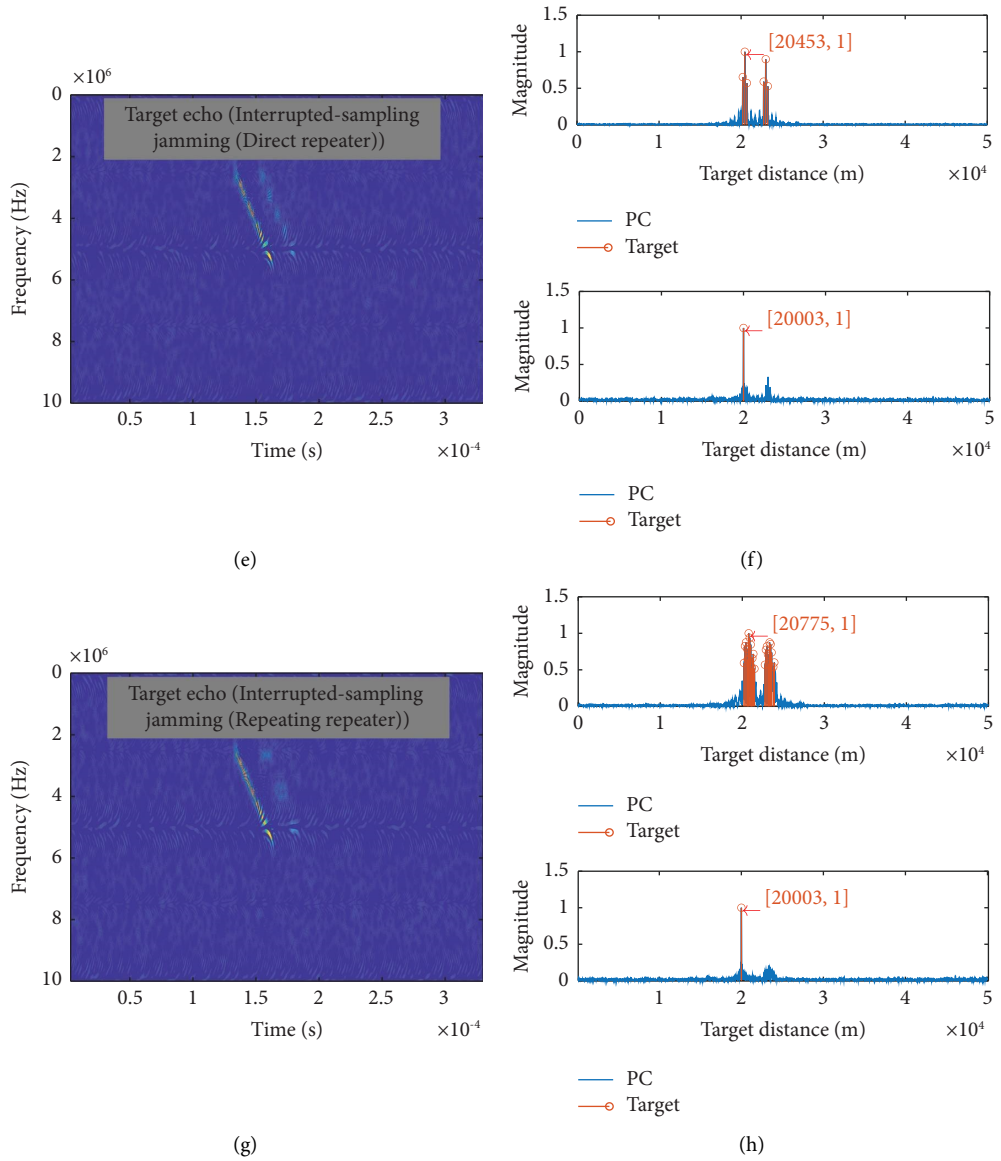

Figure 3: (a, c, e, g) The time-frequency distributions of the extracted signals by the proposed method. (b, d, f, h) The comparison of pulse compression results before and after processing.

Table 2: The comparison of results before and after processing.

Type	SIR (dB)		The error rate of the estimated radial distance		Target number	
	Before	After	Before (%)	After (%)	Before	After
Noise convolution jamming	−15	1.48	0.015	0.015	32	1
Slicing jamming	−15	0.95	19.25	0.015	107	1
ISRJ-direct repeater	−15	6.63	2.265	0.015	6	1
ISRJ-repeating repeater	−15	−3.16	3.875	0.015	25	1

number of the pulse compression (PC) result. About the SIR after interference elimination, it can be calculated by referring to (7) and (8). Theoretically, after elimination, the energy coefficient of the interfering signal is 0, while considering the estimation error of $\mathbf{A}$, the energy coefficient of the interfering signal should be assigned by $\hat{\mathbf{A}}_{inv}^{ij} \cdot \mathbf{A}$, where $\hat{\mathbf{A}}_{inv}^{ij}$ is a submatrix of the estimated observed matrix $\hat{\mathbf{A}}$.

As shown in Figure 3 and Table 2, the target echo could still be extracted effectively under the overlapping with different interfering signal types, and SIR gets promoted by at least 12 dB versus that before processing, and the false targets

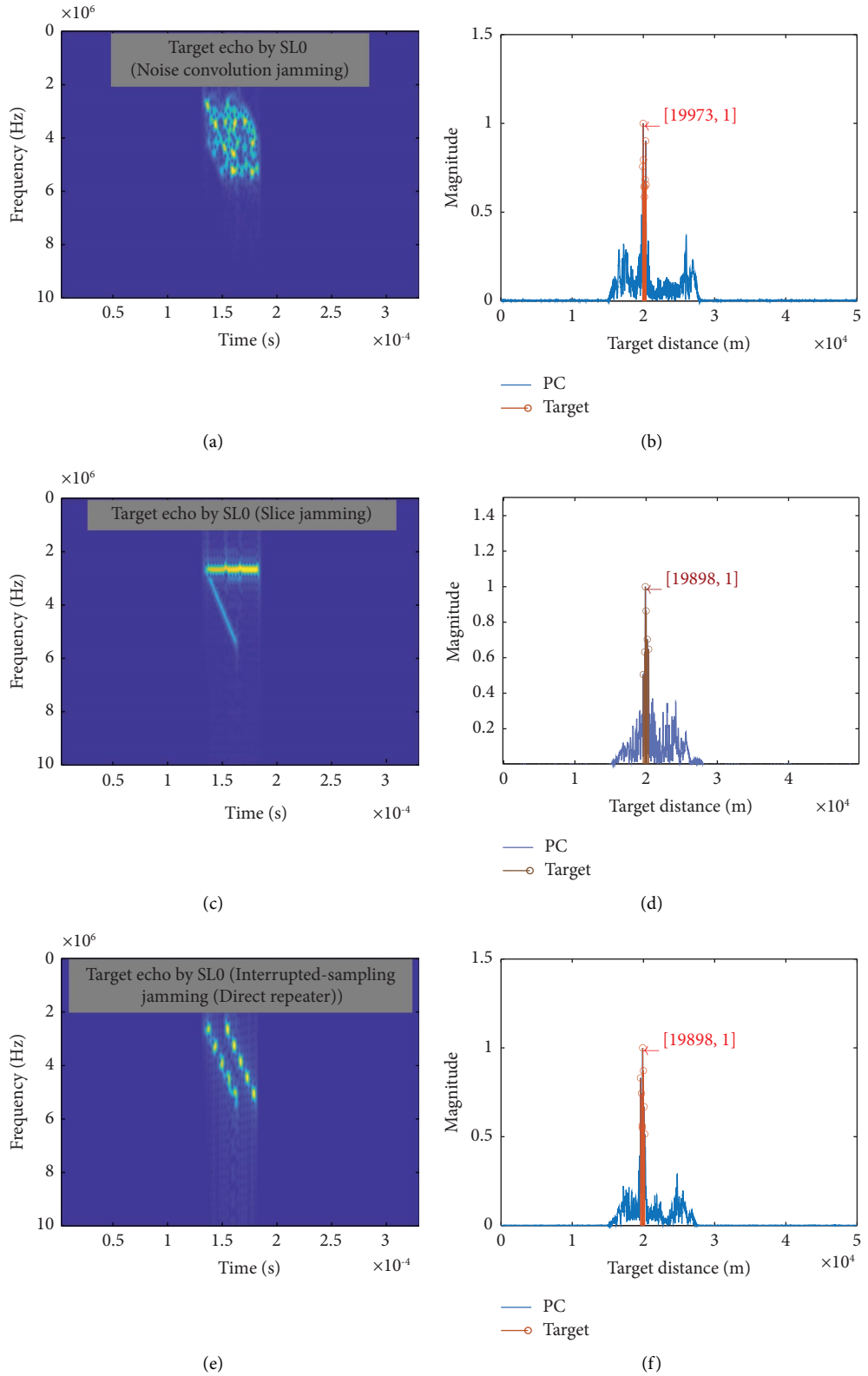

Figure 4: Continued.

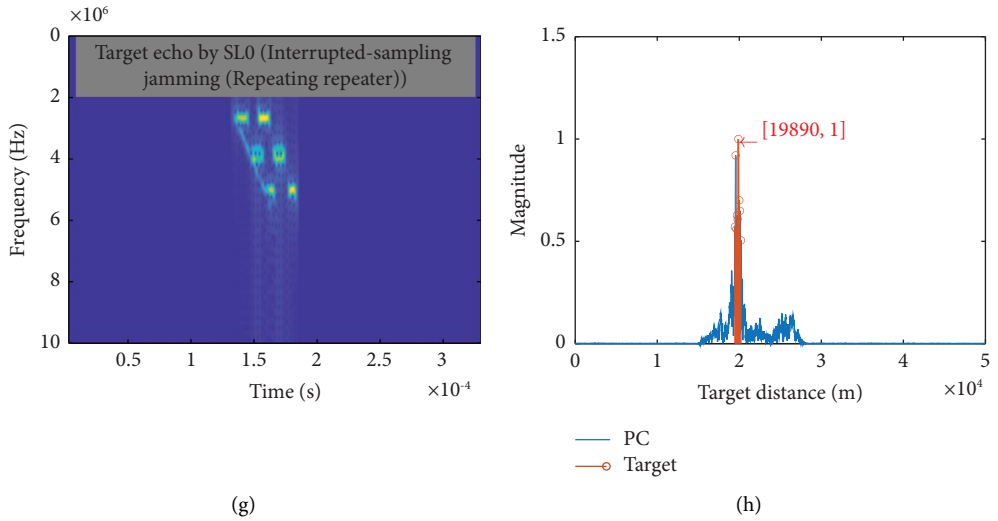

Figure 4: (a, c, e, g) The time-frequency distributions of the extracted signals by the SL0-based method. (b, d, f, h) The pulse compression results after processing by the SL0-based method.

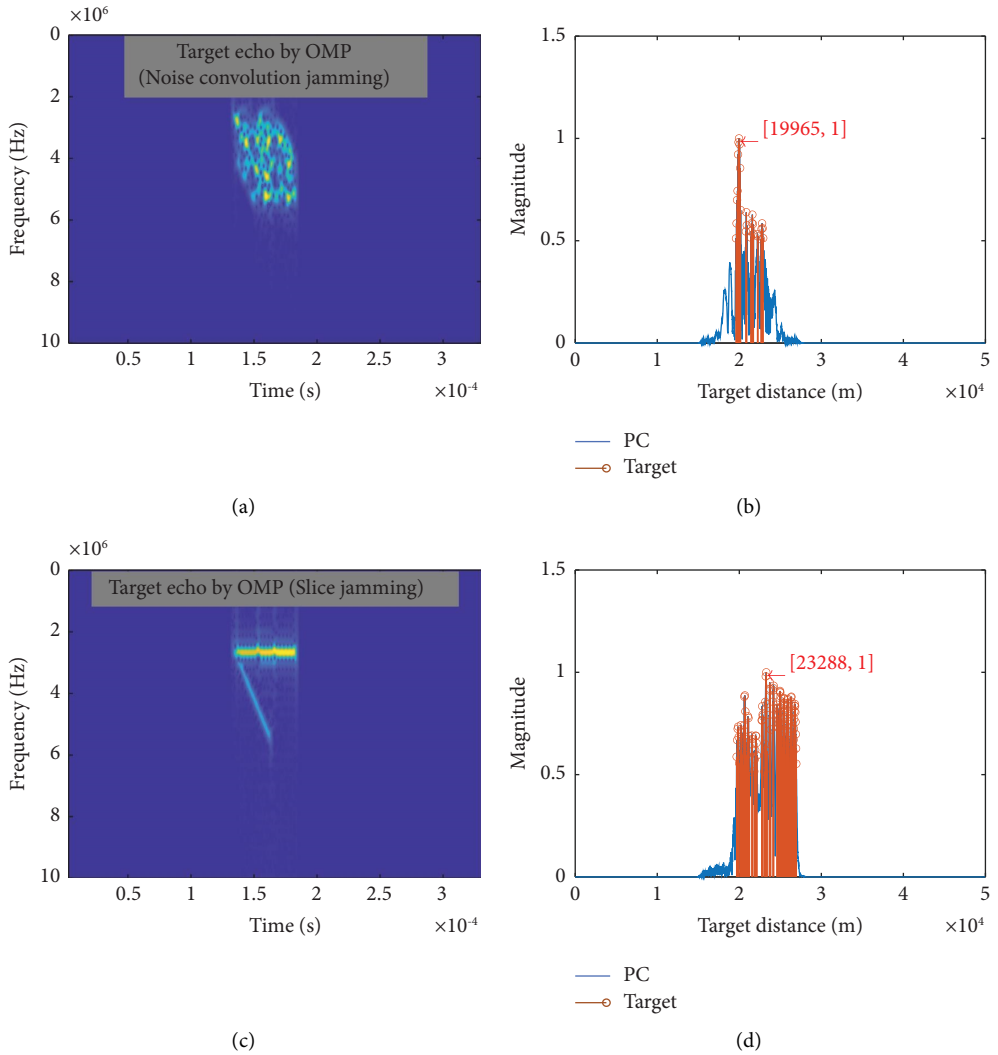

Figure 5: Continued.

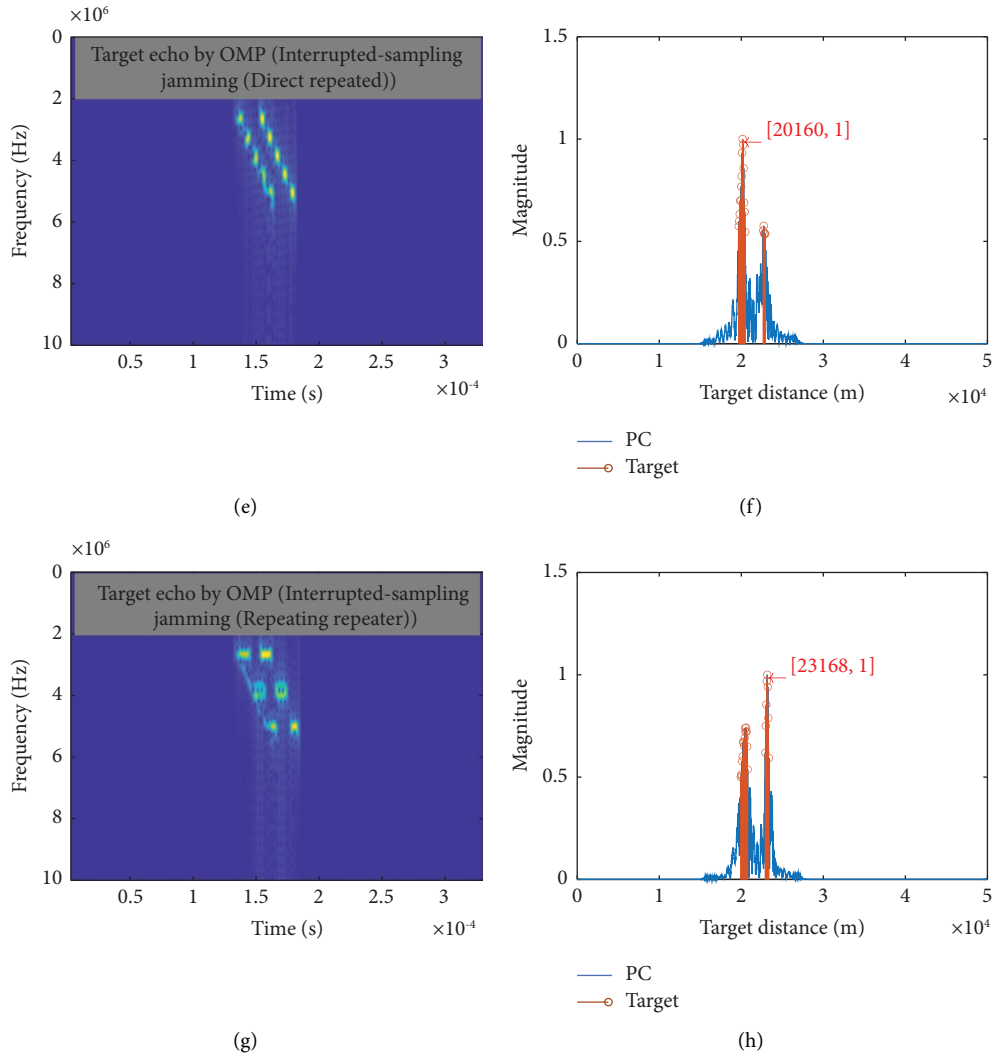

FIGURE 5: (a, c, e, g) The time-frequency distributions of the extracted signals by the OMP-based method. (b, d, f, h) The pulse compression results after processing by the OMP-based method.

are completely removed. While the target echo is still affected by the additive noise to a certain degree, showing slight distortion in the time-frequency distribution, from the result of pulse compression, the noise influence is almost negligible.

3.3. Test 2. Here, two conventional source recovery methods based on SCA are used in this study, namely the SL0-based and OMP-based methods [20, 21]. In comparison to our method, they are used to process hybrid signals in the time-frequency domain uniformly, where SJR = −15 dB and SNR = 0 dB.

In Figures 4 and 5, with the time-frequency overlaps being existed, the interfering signal can hardly be suppressed by the selected methods, and what follows is that the actual target information is still unavailable. However, the effect of those two methods appears to be superior in terms of denoising.

For intuitive comparison, the quantitative pulse compression results and computational complexity under different methods are given in Table 3. As can be seen, in terms of pulse compression, the error rates of estimated radial distance of the SL0-based and OMP-based methods are still high, and the false targets still exist in the majority of cases, whose performances are much lower than that of the proposed method. As for the computational complexity, the SL0-based and OMP-based methods mainly contain the seeking of the inversion of the entire time-frequency matrix; hence, their computational complexities are equal to $O(n^2)$. While in the proposed method, we just need to seek the inversion of the mixing observed matrix, and the rest operations are mostly linear, since the complexity could be $O(n)$.

As a result, the proposed method outperforms the selected conventional methods in terms of interference elimination and computational complexity. Simultaneously,

Table 3: The comparison of results under different methods.

Method	Computational complexity	Type	The error rate of estimated radial distance (%)	Target number
SL0-based	$O(n^2)$	Noise convolution jamming	0.135	9
		Slicing jamming	0.51	6
		ISRJ-direct repeater	0.51	8
		ISRJ-repeating repeater	0.55	9
OMP-based	$O(n^2)$	Noise convolution jamming	0.175	26
		Slicing jamming	16.44	135
		ISRJ-direct repeater	0.8	19
		ISRJ-repeating repeater	15.84	23
Proposed	$O(n)$	Noise convolution jamming	0.015	1
		Slicing jamming	0.015	1
		ISRJ-direct repeater	0.015	1
		ISRJ-repeating repeater	0.015	1

it is known that the slice jamming and ISRJ-repeating repeater exhibit superior interference performance, which is consistent with the findings of most similar studies.

4. Conclusion

To address the new coherent jamming's countermeasure, this paper first summarizes the primary characteristics of the new coherent jamming and the basic principle of the current mainstream countermeasures and then proposes an interference elimination method based on signal feature transformation (SFT). The mainstream countermeasures generally rely on identifying the conventional signal feature differences to complete target echo extraction, while we transform the antijamming problem here into a linear underdetermined blind source separation model and solve it by transforming the signal features of the observed information in the time-frequency domain. Simulations demonstrate that the proposed method is feasible, and the SIR of the output gets much improvement versus that before processing. Compared with the mainstream countermeasures, it has obvious advantages, particularly in the estimation of target radial distance and false target removal. Finally, future work will focus on the suppression of coherent jamming in a single channel.

Data Availability

The data that support the findings of this study are available from the corresponding author upon reasonable request.

Conflicts of Interest

The authors declare that they have no conflicts of interest.

References

[1] Lu Wang, *Research on novel active jamming suppression technology for radar*, University of Electronic Science and Technology of China, Chengdu, China, 2019.

[2] M. Ge, G. Cui, and L. Kong, "Mainlobe jamming suppression for distributed radar via joint blind source separation," *IET Radar, Sonar & Navigation*, vol. 13, no. 7, pp. 1189–1199, 2019.

[3] Z. Xiang, B. Chen, and M. Yang, "Transmitter polarization optimization with polarimetric MIMO radar for mainlobe interference suppression," *Digital Signal Processing*, vol. 65, pp. 19–26, 2017.

[4] L. Rongfeng, "combining Sum-difference and auxiliary beams for adaptive monopulse in jamming," *Journal of Systems Engineering and Electronics*, vol. 24, no. 3, pp. 372–381, 2013.

[5] H. J. Zhao, X. W. Yang, and L. H. Zhang, "A main lobe interference suppression method based on sum and difference beam for digital array radar," *Guidance & Fuze*, vol. 38, no. 2, pp. 30–33, 2017.

[6] S. Xi, *Research and implementation of repeater jamming countermeasure algorithm for LFM pulse radar*, Nanjing University of Science and Technology, Nanjing, China, 2017.

[7] X. Liu, J. Luo, and W. Wang, "Adaptive detection of phase quantized DRFM deception jamming," *Journal of Data Acquisition & Processing*, vol. 30, no. 6, pp. 1302–1309, 2015.

[8] X. Zhang, *Research on anti-jamming and target detection of mimo radar based on polarization diversity and frequency diversity*, Xi'an University of Electronic Science and Technology, Xi'an, China, 2019.

[9] L. Xu, *Research on radar waveform design and techniques against main lobe active jamming*, Xi'an University of Electronic Science and Technology, Xi'an, China, 2019.

[10] Z. Liu, L. Li, and Z. Zheng, "Mixing matrix estimation method for dual-channel time-frequency overlapped signals based on interval probability," *ETRI Journal*, vol. 41, no. 5, pp. 658–669, 2019.

[11] J. Sun, Y. Li, J. Wen, and S. Yan, "Novel mixing matrix estimation approach in underdetermined blind source separation," *Neurocomputing*, vol. 173, no. 3, pp. 623–632, 2016.

[12] L. Stankovic, I. Orovic, S. Stankovic, and M. Amin, "Compressive sensing based separation of nonstationary and stationary signals overlapping in time-frequency," *IEEE Transactions on Signal Processing*, vol. 61, no. 18, pp. 4562–4572, 2013.

[13] H. Mohimani, M. Babaie-Zadeh, and C. Jutten, "A fast approach for overcomplete sparse decomposition based on smoothed L-0 norm," *IEEE Transactions on Signal Processing*, vol. 57, no. 1, pp. 289–301, 2009.

[14] R. Qi, Y. Zhang, and H. Li, "Overcomplete blind source separation based on generalized Gaussian function and SL0 norm," *Circuits, Systems, and Signal Processing*, vol. 34, no. 7, pp. 2255–2270, 2015.

[15] J. Feng and X. Zhang, "Block sparse signal reconstruction algorithm based on improved smooth L0 norm," . *computer knowledge and technology*, vol. 15, no. 79, pp. 3–10, 2019.

[16] Y. Qiu, C. Sun, and J. Tang, "Seismic attribute fusion approach using optimized fastICA-based blind source separation algorithm," *Geophysical Prospecting for Petroleum*, vol. 57, no. 5, pp. 733–743, 2018.

[17] Y. Chen, *Research on blind communication signals extraction technology based on improved independent component analysis with reference algorithm*, Zhengzhou University, Zhengzhou, China, 2016.

[18] W. L. Hwang, K. S. Lu, and J. Ho, "Constrained null space component analysis for semiblind source separation problem," *IEEE Transactions on Neural Networks and Learning Systems*, vol. 29, no. 2, pp. 377–391, 2018.

[19] Z. Liu, L. Wang, Y. Feng, Z. Qian, X. Xu, and X. Chen, "A recognition method for time-frequency overlapped waveform-agile radar signals based on matrix transformation and multi-scale center point detection," *Applied Acoustics*, vol. 175, Article ID 107855, 2021.

[20] Y. Shen and S. Li, "Sparse signals recovery from noisy measurements by orthogonal matching pursuit," *Inverse Problems and Imaging*, vol. 9, no. 1, pp. 231–238, 2015.

[21] J. Feng, G. Zhang, and F. Wen, "Improved sparse signal reconstruction algorithm based on SL0 norm," *Journal of Data Acquisition & Processing*, vol. 31, no. 1, pp. 178–183, 2016.